Ultrathin Au films on W(110): Epitaxial growth and electronic structure

H. Knoppe and E. Bauer
Physikalisches Institut, Technische Universität Clausthal, D-38678 Clausthal-Zellerfeld, Federal Republic of Germany
(Received 1 March 1993)

Gold films between 1 and 11 monolayers in thickness were prepared on W(110) by molecular-beam epitaxy at substrate temperatures between 180 and 550 K. Thickness and quality of the growing films were characterized with reflection high-energy electron diffraction, Auger-electron spectroscopy, and, in particular, with He I excited angle-resolved ultraviolet photoelectron spectroscopy, which was also used for the study of the electronic structure of the films. The initial quasi-monolayer-by-monolayer growth mode leads to pronounced thickness-dependent changes of the Au electronic states. Quantum-well states derived from the Λ_6 band of Au are observed for thicker films before the spectra become identical to those well known from bulk Au(111).

I. INTRODUCTION

The electronic structure of ultrathin films differs strongly from that of the bulk. This is particularly evident in the chemical properties[1] and in the magnetic behavior.[2] In the monolayer limit[3] the lattice periodicity perpendicular to the film is lost and, neglecting interaction with the substrate, the electronic structure of monolayer and double layer films is truly two dimensional. The interaction with the substrate strongly modifies the two-dimensional band structure. Even for thicker films significant deviations from the bulk electronic structure have to be considered due to the quantization of the perpendicular wave number $k_\perp$, i.e., the occurrence of the quantum size effect (Refs. 4–7 and references therein).

The main factors which determine the electronic structure of a thin film in contact with a substrate are thickness, symmetry, and packing density of the film and its electronic interaction with the substrate. The goal of this study is to shed some light on the importance of these factors for the specific system Au on W(110). Au is a much studied $5d$ band metal. It has, for example, interesting surface reconstructions[8–10] and is used for nonmagnetic spacer layers in Co-Au superlattices.[11] The bulk band structure of Au is well known,[12–14] so that the transition from two to three dimensions can be studied.

Up to now the electronic structure of Au films has been investigated with electron reflection spectroscopy on Ni, Pd, and Ag substrates[15] and with photoemission techniques on some metallic substrates such as Ag,[16] Nb,[17] Ru,[18,19] as well as Al, Cu, Pd, Pt, and W (see Ref. 3 and references therein), and on semiconducting substrates such as Si,[20] Ge,[21] and GaAs,[22] but often with low energy and/or angular resolution. Furthermore, Au tends to form monolayer alloy films with Al, Cu, and Pd,[3] and the layer-by-layer growth mode of Au on Ag(111) is still under discussion.

For the present study the (110) face of tungsten was chosen as substrate, (i) because W(110) is a smooth surface on an atomic level and has a high surface energy, which is a prerequisite for initial two-dimensional growth[23] and (ii) because W has a low density of states in the energy region of the Au $5d$ bands, which makes a clear separation of the Au thin film states from the W $5d$ states possible. The growth mode of Au on W(110) and of the closely related system Au on Mo(110) has been investigated in several studies.[24–28]

II. EXPERIMENT

The experimental setup has been described in detail previously.[29–31] Therefore, we restrict ourselves here to its most important features. The UHV system consists of a VG Instruments, Inc. VG-ESCALAB spectrometer with a 150 mm radius hemispherical analyzer. The spectrometer is connected via a 70 mm diameter tube with a reflection high-energy electron diffraction (RHEED) chamber. A fast entry air-lock allows easy sample exchange. The lowest temperature accessible with the exchangeable specimen holder is 180 K instead of the 100 K used earlier.[29,30]

The RHEED system was used to determine the structure, the growth mode, and the deposition rate. Details may be found elsewhere.[32] In the RHEED chamber Au was evaporated from a W crucible heated by electron bombardement and deposited at normal incidence at rates up to 1 monolayer (ML) per minute. During deposition the pressure stayed below 8×10^{-9} Pa.

For angle-resolved ultraviolet photoelectron spectroscopy (ARUPS) the He I line ($h\nu = 21.22$ eV) from a Leybold capillary discharge lamp was used. The energy resolution of the analyzer was set to 100 meV; the angular acceptance was $\pm 1°$. The polar angle Θ of emission of the photoelectrons was set by rotating the sample which could also be rotated azimuthally. The normal emission measurements presented in this study were made with unpolarized light incident in the W $(1\bar{1}0)$ mirror plane at 36° from the sample normal.

For Auger-electron spectroscopy (AES) a 1.8 keV, 3 μA electron beam was used and the angular acceptance of

the analyzer was set at ±12°. The Auger signal was differentiated by modulation of the target potential with 5 V_{pp} for the detection of impurities and 1 V_{pp} for *in situ* monitoring of the film growth.

In the spectrometer chamber Au was evaporated from a ceramic crucible, which was resistively heated by a tungsten coil. After careful outgassing a working pressure of less than 6×10^{-9} Pa was reached at deposition rates of 0.1 ML per minute. The W sample was cleaned with the usual procedures until no contamination was detectable (C:W, O:W AES signal ratio 1:300). Only small amounts of oxygen could be detected (O:W about 1:100) after extended measurement periods of more than 12 h, still without noticeable influence on the ARUPS spectra.

For ARUPS measurements up to temperatures of 600 K the sample was heated by thermal radiation from resistively heated W filaments below the sample holder. The heating current was chopped periodically with a period of 60 ms of which 20 ms were off in order to eliminate magnetic fields during the measurement. The emf of a W-Re thermocouple spotwelded to the edge of sample was used for temperature stabilization via filament current regulation. The absolute accuracy of the temperatures given is ±20 K.

The ARUPS data were collected continuously during Au deposition at very low deposition rates of about 1 monolayer per hour. This allowed us to determine with one deposition the complete energy and coverage dependence of the intensity of the photoemission features.

For a higher coverage resolution of certain ARUPS features, only the intensities at several fixed energies were measured quasisimultaneously during Au deposition by switching the analyzer energy typically every 2 s between the different interesting energies.

III. RESULTS

A. Film structure and growth mode

For our studies we need atomically smooth Au films with well-defined thickness and crystalline structure. The latter has been investigated in detail before at and above room temperature.[24,25] Briefly, the results important for us show that the monolayer and the double layer films on W(110) consist of slightly distorted close-packed Au(111) layers rotated towards the Kurdjumov-Sachs orientation, where the close-packed Au [1$\bar{1}$0] atomic rows are parallel to the W [1$\bar{1}$1] and [$\bar{1}$11] directions, resulting in the formation of two domains.[24] The angle of rotation between the Au [11$\bar{2}$] and the W [1$\bar{1}$0] azimuth is less than 2.5°, so that the deviation from the higher symmetry Nishiyama-Wassermann orientation, which has only one domain with Au [11$\bar{2}$] || W [1$\bar{1}$0], is rather small. Thick films show the low-energy electron diffraction pattern of Au(111),[25] whose surface layer is known to reconstruct laterally in a herringbone like pattern.[8–10]

With RHEED we have studied the quality of Au films grown both at and below room temperature. The RHEED pattern of films with thicknesses of about 10 ML is similar to the Au(111) pattern of Ref. 33, which also reveals the reflections due to the surface reconstruction. Figure 1 shows the oscillations of the specular RHEED beam intensity during the deposition of Au on W(110) at about 180 K (upper curve) and at room temperature (300 K, lower two curves). The constant period after the fourth maximum was attributed to the deposition of 1 ML.[34] The 180 K curve shows regular oscillations with smaller damping than at 300 K. Similar to other metal on metal systems, this is due to a faster approach to the steady state of terraces and steps at 300 K.[31,32] At reduced temperature the nucleation rate is higher and the diffusion length is smaller, so that the surface is becoming rough on the 1–10 nm scale.

The shape of the first two periods at 300 K in Fig. 1 differs from the regular ones seen at larger coverages and those at 180 K. At 0.25° glancing angle (second curve, Fig. 1) the initial periods consist of broad maxima followed by rather sharp minima. At somewhat larger angles (0.65°, bottom curve) two maxima occur between 1 and 2 ML and the first monolayer maximum becomes asymmetric with a sharp intensity drop. It is interesting to note, that for perfect layer-by-layer growth dynamical calculations of RHEED intensity oscillations at small glancing angles yield a sharp decrease of intensity when a new monolayer starts to grow.[35] Regular and damped oscillations develop if several monolayers grow at the same time. Measurements of the homoepitaxial growth of Pb-In alloy films showed that the shape of these "extra maxima" strongly depends upon the azimuthal angle.[36] The curves with the incident beam parallel to the [1$\bar{1}$0] azimuth of Pb are comparable to the double maximum mentioned above (Fig. 1), where the incident beam direction was the [001] azimuth of W which is nearly parallel to [1$\bar{1}$0] of Au.[24] Because the atomic numbers of Pb and Au and, therefore, their atomic scattering factors are comparable, we conclude that the first two layers of Au on W(110) grow quasi-two-dimensional at 300 K. The intensity drops starting at about 0.85 and 1.85 ML indicate the formation of 2 and 3 ML thick islands before the first and second monolayer, respectively, are completed. At 180 K, however, several monolayers grow simultane-

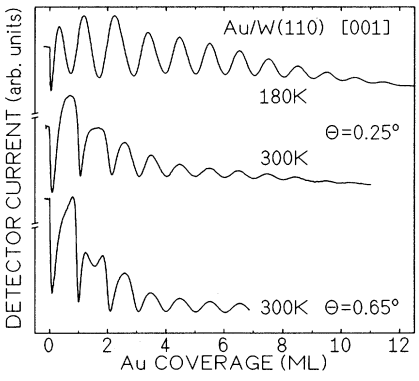

FIG. 1. Intensity oscillations of the specular RHEED beam during the growth of Au on W(110) at 180 K (upper curve) and at room temperature (300 K, lower two curves). The [001] azimuth was in the plane of incidence, the glancing angle was 0.25° and 0.65° (upper two curves and bottom curve, respectively), and the primary energy was 15 keV.

ously, not only at larger thicknesses as was seen from the damping of the oscillations, but from the beginning.

Another common method for the determination of the growth mode of ultrathin films is the analysis of the development of the Auger-electron signals. Figure 2 shows the amplitude of the differentiated Auger-electron signal of Au vs deposition time in normal emission. The obvious slope change at 13.5 min is attributed to the completion of the first Au monolayer (upper axis in Fig. 2). The absence of a second slope change at 2 ML has to be analyzed with care, because the inset in Fig. 2 shows that there is a considerable change in the Auger-electron peak shape between 1 and 3 ML. This effect has been discussed before for Au on Mo(110).[27] These measurements and others for Au on W(110) (Ref. 25) were made with a cylindrical mirror analyzer at an emission angle of 42°. The curves are very similar to Fig. 2 taken at 0°. This dependence on the angle of Auger-electron emission confirms that the lack of the double layer break is caused by changes in the electronic structure of the Au films and not by diffraction effects, which can lead to angular-dependent slope changes in the Auger curves.[31]

The ARUPS intensities themselves may be used for the analysis of the film growth mode, because of the small escape depth of the He I excited photoelectrons and the drastic changes of the electronic structure with film thickness. Figure 3 shows ARUPS spectra from the clean W(110) surface, and from 0.7, 1.0, and 2.0 ML thick Au films deposited at room temperature. The spectra were taken in normal emission; the initial energy E refers to the Fermi level E_F.

Figure 4 shows the development of the ARUPS intensities measured quasisimultaneously at three different energies during continuous deposition of Au on W(110) at 550 K. Here the completion of the first and second monolayer can be seen unambiguously in the maxima of the curves taken at −3.18 and −2.61 eV, respectively, which are the positions of the dominating 1.0 and 2.0 ML peaks in Fig. 3. Up to 2.5 ML the curves consist of straight segments with very sharp slope changes at 1 and 2 ML. The deviations of the curves from linearity above 2.5 ML indicates that the third monolayer is not completed at 550 K due to the transition to the Stranski-Krastanov growth mode, which occurs at the elevated temperature used here in the third monolayer.

The weak change of slope of the −3.18 eV curve in Fig. 4 at about 0.8 ML is due to the small shift in the position of the dominating monolayer peak seen in the spectra of 0.7 and 1.0 ML (Fig. 3). Spectra taken at 500 K in steps of 0.07 ML (compare Sec. III B) showed that this peak shift occurs only between these two coverages. Below 0.7 ML and above 1.0 ML the peak near −3.2 eV does not change its position. From 0.7 to 1.0 ML another small peak shift occurs at about −4.15 eV in Fig. 3. Both shifts suggest minor changes in the structure of the first mono-

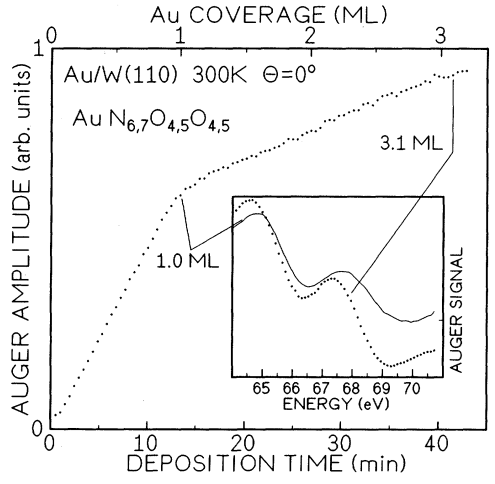

FIG. 2. Deposition time and coverage dependence (lower and upper axis, respectively) of the Au Auger intensity during continuous deposition of Au on W(110) at 300 K. The inset shows the differentiated signal of the Au $N_{6,7}O_{4,5}O_{4,5}$ Auger electrons for the coverages 1.0 and 3.1 ML. The peak-to-peak amplitude was measured between the maximum and the minimum at about 65 and 69 eV, respectively.

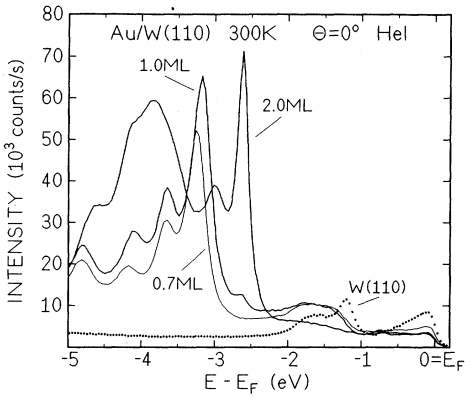

FIG. 3. Normal-emission ARUPS spectra from the clean W(110) substrate and from 0.7, 1.0, and 2.0 ML of Au deposited on W(110) at room temperature. E_F denotes the Fermi level.

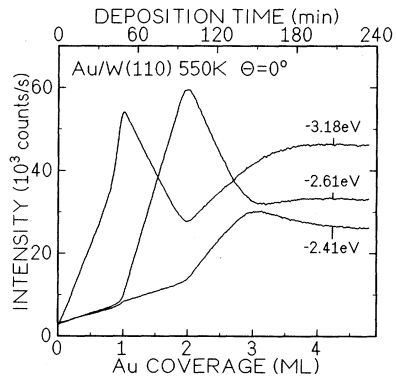

FIG. 4. Normal-emission ARUPS intensities at initial energies E with respect to the Fermi level, as indicated, vs coverage and time (lower and upper axis, respectively) during continuous deposition of Au on W(110) at 550 K.

layer which are undetectable in the electron diffraction pattern. The change of slope in the −3.18 eV curves occurs earlier (0.7 ML) in room-temperature measurements than at 550 K (Fig. 4). Annealing of 1.0 ML thick films up to more than 800 K yields again the peak position found below 0.7 ML. Thus, the structure observed below 0.7 ML is the thermodynamic equilibrium structure also above 0.7 ML up to 1.0 ML. Kinetic limitations suppress it above 0.7 ML at room temperature and above 0.8 ML at 550 K.

The curves in Fig. 5 were taken at room temperature at the energies −3.21 and −2.64 eV which are similar to those in Fig. 4 characteristic of 1 and 2 ML, respectively, and at −4.18 eV, which is the position of a Au(111) surface resonance[13,14] which saturates at 4 ML Au on W(110) (see below). The arrows in Fig. 5 mark breaks in the deposition at which the film was annealed at 870 K (1 ML) and at 550 K (2 ML). At room temperature the second and third monolayer start to grow before the first and the second layer, respectively, are completed. This can be seen from the deviations from linear behavior of the corresponding curves in Fig. 5 and from the 1 ML room-temperature spectrum shown in Fig. 3, which shows already the −2.6 eV peak due to 2 ML thick islands. Annealing smoothes the film, and thus, the photoemission intensities of the −3.21 and −2.64 eV curves increase at 1 and 2 ML (upward arrows) and decrease at 2 and 1 ML (downward arrows), respectively. In contrast, the Au(111) surface resonance curve (−4.18 eV) is almost linear with little response to the annealing.

The rapid decrease of the intensity of the maxima at 1 and 2 ML in Fig. 5 for a short period after the restart of the Au deposition can be understood by single Au atoms on atomically smooth terraces, in this case, which suppresses the monolayer, respectively, double layer peaks stronger than the same number of Au atoms nucleated in two-dimensional islands. The end of the sharp decrease, thus, signals two-dimensional nucleation.

Summarizing, the ARUPS measurements clearly indicate almost perfect layer-by-layer growth of Au on W(110) up to 2.5 ML at elevated temperature (550 K).

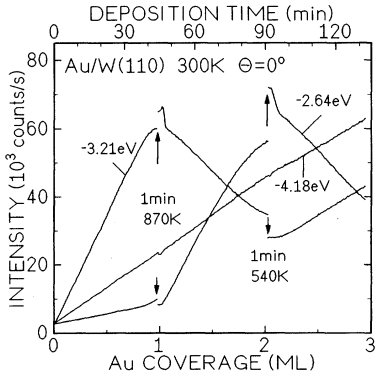

FIG. 5. Same as in Fig. 4 but for deposition at 300 K. The arrows mark deposition pauses with 1 min annealing at 870 K (1 ML) and at 540 K (2 ML) followed by cooling to 300 K before continuation of Au deposition.

Films grown at room temperature can be smoothed by annealing. Films thicker than 2.5 ML should be grown at 300 K to prevent roughening due to the increasing tendency to Stranski-Krastanov growth mode with increasing temperature. On the other hand, as indicated by the RHEED results, films grown at low temperature (180 K) become rough from the first monolayer on due to the higher nucleation rate and smaller diffusion length compared to 300 K.

B. Normal-emission ARUPS: Observation of quantum-well states

An overview of the development of the electronic structure with film thickness was obtained by measuring normal-emission ARUPS spectra during continuous deposition of Au with a rate of about 0.9 ML per hour at substrate temperatures of 300 and 500 K. Figure 6 shows some of these spectra close to integer monolayers from 0 up to 8 ML of Au on W(110). 25 (14) spectra were measured during the deposition of every ML at 300 K (500 K). The positions of the direct bulk transitions 2–6, the surface resonances D_1 and D_2, of the shoulder S, and of the Shockley surface state SS at −0.40 eV are marked following Ref. 14 for comparison with the He I excited Au(111) spectrum, which is very similar to the spectrum of 8 ML of Au on W(110) at 300 K [Fig. 6(a)].

At 300 K differences are found in the structures at the shoulder S, in the better resolution of the direct transitions 5 and 6 in our case, and in the position of the surface state, which is seen from 4 ML on upward[37] at −0.45 eV. Only after annealing of room-temperature deposited films or at 500 K [Fig. 6(b)] its energy is −0.40 eV.

A comparison of the spectra of 1 and 2 ML with those from Au(111) (8 ML) shows the drastic influence of the film thickness. From 3 ML on upward the bulk transitions 2–4, the surface state, and the strong surface resonances D_1 and D_2 can be identified with almost unchanged energy. The intensities of D_1 and D_2 saturate at about 4 and 6 ML, respectively, those of the bulk transitions still increase at 8 ML, both at 300 and 500 K.

At 500 K [Fig. 6(b)] the spectra with more than 2 ML thickness are smeared out more than those taken at 300 K. Even after cooling the 8 ML thick film to room temperature, the bands 5, 6, and the structures at the shoulder S were not as well resolved as in Fig. 6(a), indicating the increased tendency to the Stranski-Krastanov growth mode at elevated temperature which leads to a rough surface.

The energy positions of the features identified in the spectra in Fig. 6(a) between −4 and −2 eV are plotted vs coverage in Fig. 7. The bulk transitions 5 and 6 do not shift much between 6 and 11 ML, but the structures closer to the shoulder S show a systematic trend towards higher energy, which is characteristic of quantum-well states. The lines labeled $n = 1,\ldots,4$ represent a fit to these data, which will be described below.

The detailed coverage dependence of the intensities measured between −3.21 and −2.25 eV is shown for every second measured energy step in Fig. 8. The rather broad maxima from 3 ML on upward are attributed to

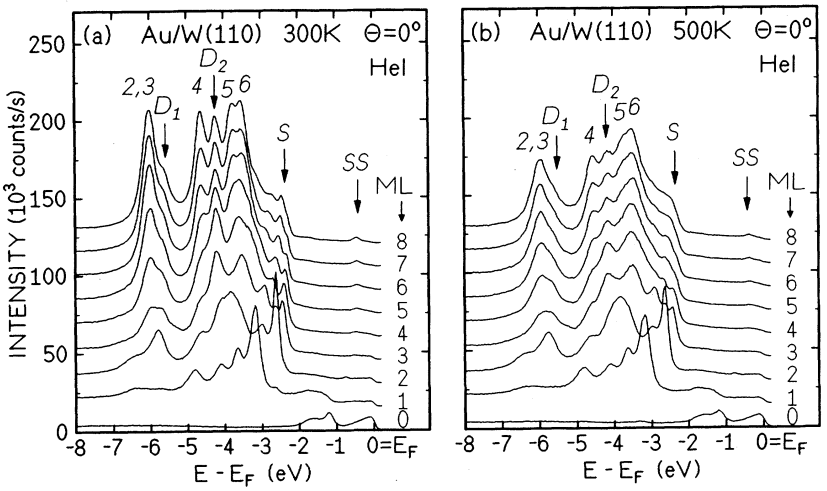

FIG. 6. Normal-emission ARUPS spectra for Au coverages from 0 to 8 ML measured during continuous deposition of Au on W(110) at room temperature (a) and at 500 K (b). The Au(111) surface state SS, the shoulder S, the surface resonances D_1 and D_2, and the direct bulk transitions 2–6 along ΓL for He I excitation ($h\nu = 21.22$ eV) are marked following Ref. 14. For clarity the curves are shifted vertically in increments of 20×10^3 counts/s.

quantum-well states. At lower coverages the behavior is dominated by the quasi-monolayer-by-monolayer growth mode.

In the simplest view of a quantum well as an interferometer of Fabry-Pérot geometry[4] one expects the resonant states to appear at fixed energy E at film thicknesses $d_n(E)$ spaced by a period $\lambda/2$. The phase condition for constructive interference of the electron wave, which is multiply reflected at the potential barriers of the film-vacuum and film-substrate interface with a total boundary phase shift $\delta(E)$, is[7]

$$2\,k(E)\,d_n(E) + \delta(E) = 2n\pi \quad . \tag{1}$$

Quantum-well states derived from bulk bands close to Brillouin-zone boundaries[4,7,38] consist of an envelope function to the Bloch states at the zone boundary which satisfies Eq. (1) and which is formed by the superposition of the equivalent Bloch waves $k_\perp(E) = \pi/d_0 \pm k(E)$. Therefore, two states n and $n+1$ with the same energy E and with film thicknesses d_n and d_{n+1} differing by p monolayers of thickness d_0 yield the following relation:[4]

$$k_\perp(E) = \frac{\pi}{d_0}\left(1 \pm \frac{1}{p(E)}\right) \quad . \tag{2}$$

We measure $p(E)$ between the states $n = 1$ and 2 and between 2 and 3 in Fig. 7 from 3 and 4 ML, respectively, on upward. At lower coverages the changes in energy are rather irregular. Figure 9 compares the values of $k_\perp(E)$ obtained this way with the experimentally determined Λ_{45} d and Λ_6 s,p bands of Au(111) along ΓL.[13]

The second quantity which can be extracted from two states n and $n+1$ at the same energy E in Fig. 7 is the phase shift $\delta(E)$ (Ref. 39) which is calculated according to Eq. (1) from the ratio of the film thicknesses:

$$\delta(E) = 2\pi\left[n - \left(\frac{d_{n+1}(E)}{d_n(E)} - 1\right)^{-1}\right] \quad . \tag{3}$$

The phase is shown with a parabolic fit to the data in Fig. 10. The lines $d_n(E)$ ($n = 1, \ldots, 4$) in Fig. 7 were calculated from Eq. (1) with a linear fit of the Au on

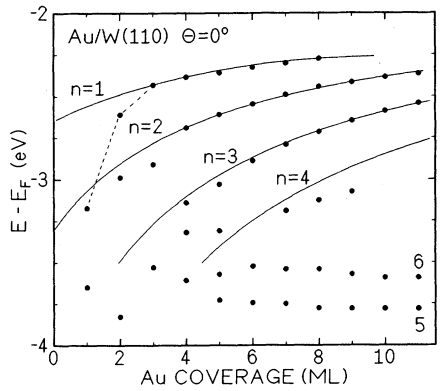

FIG. 7. Coverage dependence of the energy of the features between −4 and −2 eV in the spectra of Fig. 6(a). The lines labeled $n = 1, \ldots, 4$ represent a fit to the quantum-well states (see text).

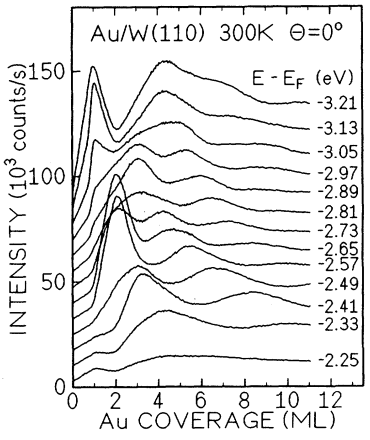

FIG. 8. Development of the ARUPS features of Fig. 7 with Au coverage in the energy range from −2.25 eV to −3.21 eV, as indicated. The curves are shifted vertically for clarity in increments of 7.5×10^3 counts/s. Note that the spectra shown in Fig. 6(a) belong to the same Au deposition.

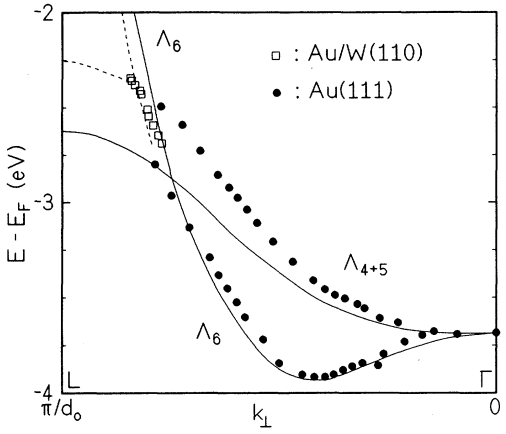

FIG. 9. $E(k_\perp)$ values (open squares) obtained from the quantum-well states of Au on W(110) (see text), experimental (full circles and dashed lines) and theoretical bands (solid lines, fitted to experiment at Γ) of bulk Au(111) from Ref. 13.

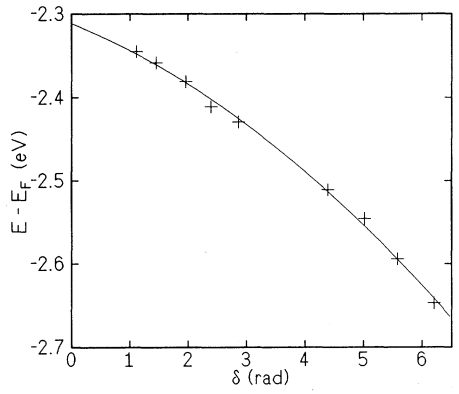

FIG. 10. Boundary phase shift $\delta(E)$ determined from the quantum-well states of Au on W(110) acccording to Eq. (3) with a parabolic fit to the data.

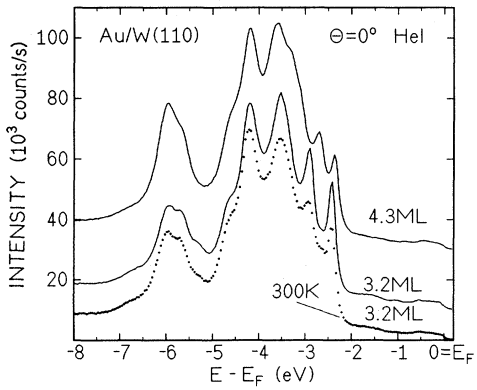

FIG. 11. Normal-emission ARUPS spectra of 3.2 and 4.3 ML Au on W(110) prepared as shown in Fig. 5 and finally annealed to 500 K for 2 min (full lines). The curves are shifted by 10 and 20×10^3 counts/s for clarity. For comparison the spectrum of 3.2 ML Au deposited at 300 K without annealing is shown (dots).

W(110) $E(k_\perp)$ data in Fig. 9 and with $\delta(E)$ as shown in Fig. 10.

Careful annealing of the films and deposition of the amount necessary to complete the monolayers exactly increases the sharpness of the quantum-well features considerably. This is clearly visible for three monolayers in Fig. 11. The 3.2 and 4.3 ML films were prepared by the procedure used in Fig. 5. Finally they were annealed for 5 min to 500 K. For comparison a 3.2 ML spectrum of a room-temperature deposited and not annealed film is shown (dots).

IV. DISCUSSION

From Fig. 7 it is evident that the validity of Eq. (1) with thickness-independent dispersion and phase relation is limited to coverages of at least 3 ML and to the $n = 1$, 2, and 3 states. The Au on W(110) $E(k_\perp)$ data in this range (open squares in Fig. 9) continue reasonably well the bulk Au(111) photoemission data of the Λ_6 band (full circles) which, in contrast to the film data, depend on the knowledge of the empty final-state band. Note that the low-energy quantum-well data deviate towards lower $k_\perp$, i.e., towards the calculated Λ_6 band.

At $h\nu = 21.2$ eV the direct transitions from the bulk bands Λ_6 and Λ_{4+5} occur close to Γ and result in the peaks 5 and 6 in the spectra.[13] Therefore, close to the L point no direct interband transitions are possible and photoemission from the quantum-well states proceeds via relaxation of the conservation rule for $k_\perp$ due to the limited inelastic mean free path of the photoelectrons.[5,40] This is also the case for the dispersionless shoulder S on which the quantum-well states appear and which is assumed to be related to the surface potential of the compressed and corrugated outermost layer of Au(111).[14]

Quantum-well states which are truly confined to the adsorbed film require the existence of a band gap within the substrate for electronic states of the same symmetry and parallel component of the wave vector which is conserved across the interface. The Au quantum-well states are of type $\Lambda_{6(1)}$ in relativistic double-group (nonrelativistic single-group) notation and can couple only to the W(110) $\Sigma_{5(1)}$ states, if spin-orbit interaction is neglected. The $\Sigma_{5(1)}$ gap ranges from -6.3 to -2.0 eV with respect to E_F, but $\Sigma_{5(2)}$ states are found between -3.4 and -2.0 eV.[41] The $\Sigma_{5(1)}$ edge is visible in the W(110) spectrum at about -2 eV (Fig. 3), which shows that the single-group character, which forbids photoemission from the $\Sigma_{5(2)}$ band,[41] dominates the transition probabilities. Therefore, also the reflectivity for the wave function of the quantum-well states should be high at the Au(111)-W(110) interface below -2 eV.

In the simple quantum-well model the phase $\delta(E)$ is a property of the barriers confining the well. The phase change in Fig. 10 of almost 2π over 0.5 eV is quite large which may be due to the proximity to the W $\Sigma_{5(1)}$ band edge and to the low energy in our case compared with other systems. The quantum-well states of noble metals on ferromagnetic substrates seen with inverse photoemission[4] have phase shifts[39] of about π between E_F and $E_F + 2$ eV. The states of Cs on Cu(111) within

0.4 eV below E_F (Ref. 6) are also close to the vacuum level due to the low Cs work function and have phase shifts of less than 0.2π. In the Ag on Cu(111) system[7] the experimental phase varies by 0.45π between -1.3 and -0.4 eV and shows a singularity at the substrate band edge. The Au on W(110) data (Fig. 10) indicate a slope of zero at about -2.2 eV, i.e., close to the W $\Sigma_{5(1)}$ band edge, but the cutoff at the Au(111) shoulder S obscures the well states or resonances at higher energies.

The deviations of the measured energies at low coverages in Fig. 7 from the predictions of Eq. (1) are due to several causes: most important the band structure $E(k_\perp)$ itself becomes meaningless in the monolayer limit due to the uncertainty of $k_\perp$. If, however, $E(k_\perp)$ is comparable to the free-electron parabola, as, for example, in Pb,[5] the monolayer quantum-well state can fit to the series of states seen at higher coverages. This is not the case for Au on W(110) due to the large disturbances by the nearby d bands. Band-structure calculations are needed to solve the question, whether the very intense and sharp monolayer and double-layer states are also Λ_6-band derived quantum-well states as seen above 3 ML or whether d electrons participate. One is tempted to link the 1, 2, and 3 ML states close to $n = 2$ in Fig. 7 with these calculated quantum-well states (full line), but then the $n = 1$ monolayer state would be missing. Therefore, the $n = 1$ states below 3 ML should be those connected by the dashed line in this figure.

The second reason for the low coverage deviations from the regular changes with film thickness is the electronic interaction with the substrate, which changes most strongly in the transition from monolayer to double layer due to the change of the coordination number. In Fig. 3 an increase in intensity is seen in the region of the W $\Sigma_{5(1)}$ band between -2 and -1.3 eV for 0.7 and 1.0 ML relative to the clean substrate and to the double layer. This is possibly due to an interface state formed by hybridization of the s,p bands of Au and W.

Furthermore, up to 3 ML (Ref. 24) the packing density and the orientation of the Au film and consequently the film-substrate interfacial properties change, which influence the crystal barrier phase shift. The structural change within the monolayer thus may cause the small shift of the dominating monolayer quantum-well peak between 0.7 ML and 1.0 ML, see Sec. III A and Fig. 3.

The sharpness of the quantum-well features decreases with film thickness due to the simultaneous growth of several monolayers at 300 K which was seen in Figs. 5 and 8 in the rounded transitions of the intensity curves from 2 ML upwards. Despite the thickness fluctuations the quantum-well states can be observed up to at least 11 ML, because at high coverages the energies of states with the same n do not change much due to thickness differences of one monolayer compared with the spacing between states with different n (see Fig. 7). The influence of the roughness of the growing film on the quantum-well features was discussed in detail for Pb.[5] On the other hand, the sharpness of the quantum-well states increases with energy because of the decreasing lifetime broadening. This can be seen by a comparison of the monolayer (-3.18 eV) with the considerably sharper double-layer state (-2.61 eV) in Fig. 3.

A comparison of the Au on W(110) normal-emission ARUPS data with those of other ultrathin Au films reveals that the influence of the substrate is very important. It can effect the electronic structure of ultrathin films by its band structure itself and by its influence on the growth mode and structure of the film.

On Al(111) an alloy is formed within the first monolayer with normal-emission ARUPS peaks at 6.0, 6.4, and 7.9 eV below E_F.[42] The next Au layer shows peaks between 4.5 and 7.5 eV. Only films more than 10 ML thick have spectra comparable to Au(111) although no diffraction pattern was observed for these films.

The ordered Au monolayer on Cu(100) forms first a $c(2 \times 2)$ structure which appears very similar to the $Cu_3Au(100)$ surface.[43] Then a $c(14 \times 2)$ hexagonal monolayer structure forms, followed by a transition to the bulk Au(111)-like electronic structure observed at 12 ML.[44] Au monolayer-induced d states were found in normal emission between 4.7 and 6.5 eV below E_F in these studies.[3] A feature is observed also near E_F in a limited photon energy range at 1 ML Au coverage which develops with increasing film thickness to the Au(111) Shockley surface state.

For 1 ML Au on Nb(110) (Ref. 17) peaks at 4.4 and 5.9 eV are reported, but neither emission angle nor angular resolution is given in this study. The normal-emission peak energies reported for 1 ML Au on Ru(0001) (2.6, 3.1, 3.6, 4.6, 6.0 eV) (Ref. 19) fall in the energy range of the Au monolayer states on W(110), but no pure Au spectrum is shown in this ARUPS study of Cu-Au monolayer alloys on Ru(0001).

Angle-integrated and x-ray-excited photoemission data give information on the density of states rather than on k-resolved states. In the studies of ultrathin Au films on Ag(111),[16] Ru(0001),[18] Pd(111),[45] W(100),[46] Pt(100), Pt(111), and Pt(997) (Ref. 47) mainly the splitting into the Au $5d_{3/2}$ and $5d_{5/2}$ components at about 6 and 4 eV below E_F is observed.

Because the bulk Cu valence bands are similar to those of Au, but with much smaller spin-orbit splitting,[12] a comparison of the electronic structure of ultrathin Au and Cu films on W(110) is interesting. Similar to Au the angle-resolved normal-emission valence-band peaks of Cu on W(110) lie close below the W $\Sigma_{5(1)}$ band edge, but the 3 main $3d$ peaks of the Cu monolayer overlap and fall within only 0.7 eV.[29] The Au 1 ML spectrum shows in addition to the quantum-well state at -3.18 eV three peaks in the Au "$d_{5/2}$" region which are well resolved (-3.63, -4.11, and -4.82 eV, see Fig. 3) and another broad feature at about -6.3 eV in the "$d_{3/2}$" region.

A second ARUPS study of Cu on W(110) includes electronic-structure calculations for one pseudomorphic Cu monolayer and shows the existence of several Cu-W interface states and Cu surface states near the zone boundary at $\bar{H}$.[48] But also near the zone-center states with more than 80% surface or interface localization are seen: one s-like band exists at about -5.2 eV in the gap along the Σ line of W mentioned above and several other bands in the region between -2.5 and -3 eV can be followed along the $\bar{\Gamma}\bar{H}$ direction. This suggests that also

the electronic states of Au on W(110) observed in normal emission in the same energy region interact little with the bulk substrate.

Cu has within the double layer a structural transition from bcc(110) to fcc(111) symmetry with large changes in packing density which clearly influence the electronic structure at fixed film thickness.[29] The same occurs for Co (Ref. 31) and Ni (Ref. 30) in the monolayer, but not for Au. The Co, Ni, and Cu states become qualitatively identical to those of the bulk material at about 4–5 ML, but the intensities still increase at this coverage. Compared with these $3d$-band metals on W(110) the Au electronic structure shows much more features in the transition from two to three dimensions which is due to the large spin-orbit splitting of Au and to the existence of the quantum-well features.

The Au monolayer d states are found generally at rather large binding energies, which supports our interpretation of the sharp and intense monolayer and double-layer peaks at -3.18 and -2.61 eV, respectively, as quantum-well states, as does the comparison of the Cu $3d$ monolayer states on W(110) with the 1 ML Au states below -3.5 eV. A reliable interpretation of the Au monolayer states on W(110) including the possibility of an interface state between -2 and -1.3 eV requires band-structure calculations for this system. At 2 ML Au on W(110) the $d_{3/2}$ and $d_{5/2}$ splitting is obvious and with the completion of the third layer already a large similarity to the Au(111) bulk electronic structure is seen, because the surface resonances D_1 and D_2 and the shoulder S are clearly found at the bulk energies. The development of the sharp direct interband transitions of bulk Au(111), however, requires film thicknesses of 6 ML (see the development of the peaks 4, 5, and 6 in Fig. 6).

V. CONCLUSIONS

The electronic structure of ultrathin monolayer and double-layer Au films on W(110) deviates strongly from that of bulk Au(111). Most important for this fact is the existence of a band gap for s,p electrons along the Σ line of W(110), which allows the formation of quantum-well states, which are intense and sharp in the first three monolayers. For films thicker than 3 ML the energy positions of these states are compatible with the bulk Au Λ_6 band. The energy separations of these states decrease with increasing coverage and their intensity decreases, but they are still visible at 10 monolayers in spite of their decreasing intensity and sharpness.

The drastic change of the ARUPS peak positions in the initial state of growth caused by adding only one monolayer of Au leads to sharp changes of slope in the intensity curves measured during Au deposition. Linear changes are connected with the two-dimensional growth of monolayer thick Au islands. Rounded transitions close to integer monolayers indicate the start of the growth of an additional layer before the preceding one is completed, which is the case at and below room temperature due to kinetic limitations. At elevated temperature initially an almost perfect layer-by-layer growth mode is seen, but the transition to Stranski-Krastanov growth occurs earlier, that is during the growth of the third layer at 550 K. Changes of slope at about 0.7 ML are caused by a structural change of the first monolayer seen in the shift of the dominating ML peak. Thus, due to the strong dependence of the electronic structure upon thickness, *in situ* ARUPS measurements can give clearer information on the growth mode than AES which relies upon attenuation. In fact, AES can become undependable in such situations.

The development of the Au(111) electronic structure with film thickness is seen clearly on W(110), because the growth mode is quasi-monolayer-by-monolayer at room temperature and because the W bands do not interact much with the Au d bands. The large spin-orbit splitting of Au compared to Ag and Cu allows a clear separation of the ARUPS features. The surface resonances of Au(111) can be identified from 3 ML on upwards at $h\nu = 21.2$ eV; the direct bulk transitions along the Λ line are seen from 4 ML on, but develop further up to about 8 ML.

ACKNOWLEDGMENTS

This study was supported in part by the Deutsche Forschungsgemeinschaft, and in part by the Volkswagen Foundation (Hannover). The authors wish to thank G. Lilienkamp and M. Jałochowski for experimental cooperation and P. Cyris for the preparation of the W sample.

[1] C. T. Campbell, Ann. Rev. Phys. Chem. **41**, 775 (1990).
[2] U. Gradmann, in *Handbook of Ferromagnetic Materials*, edited by K. H. J. Buschow (Elsevier, Amsterdam, 1993), Vol. 7, p. 1.
[3] K. Jacobi, in *Angle-Resolved Photoemission*, edited by S. D. Kevan, Studies in Surface Science and Catalysis, Vol. 74 (Elsevier, Amsterdam, 1992), p. 371.
[4] J. E. Ortega, F. J. Himpsel, G. J. Mankey, and R. F. Willis, Phys. Rev. B **47**, 1540 (1993).
[5] M. Jałochowski, H. Knoppe, G. Lilienkamp, and E. Bauer, Phys. Rev. B **46**, 4693 (1992).
[6] A. Hamawi, S. Å. Lindgren, and L. Walldén, Phys. Scr. **T39**, 339 (1991); S. Å. Lindgren, and L. Walldén, Phys. Rev. Lett. **61**, 2894 (1988).
[7] T. Miller, A. Samsavar, M. Mueller, G. Franklin, and T.-C. Chiang, Phys. Scr. **T31**, 35 (1990); M. A. Mueller, A. Samsavar, T. Miller, and T.-C. Chiang, Phys. Rev. B **40**, 5845 (1989).
[8] J. Wollschläger and N. M. Amer, Surf. Sci. **277**, 1 (1992).
[9] N. Takeuchi, C. T. Chan, and K. M. Ho, Phys. Rev. B **43**, 13 899 (1991).
[10] A. R. Sandy, S. G. J. Mochrie, D. M. Zehner, K. G. Huang, and D. Gibbs, Phys. Rev. B **43**, 4667 (1991).
[11] See Ref. 8.
[12] H. Eckardt, L. Fritsche, and J. Noffke, J. Phys. F **14**, 97 (1984).
[13] R. Courths, H.-G. Zimmer, A. Goldmann, and H. Saalfeld, Phys. Rev. B **34**, 3577 (1986).
[14] H.-G. Zimmer, A. Goldmann, and R. Courths, Surf. Sci. **176**, 115 (1986).

[15]R. C. Jaklevic, Phys. Rev. B **30**, 5494 (1984).
[16]G. K. Wertheim and D. N. E. Buchanan, Phys. Rev. B **33**, 914 (1986).
[17]M. W. Ruckman and Li-Qiang Jiang, Phys. Rev. B **38**, 2959 (1988).
[18]M. Kuhn, Z. H. Lu, and T. K. Sham, Phys. Rev. B **45**, 3703 (1992).
[19]K. Kalki, B. Pennemann, U. Schröder, W. Heichler, and K. Wandelt, Appl. Surf. Sci. **48/49**, 59 (1991); M. C. Zonnevylle, T. Rhodin, K. Wandelt, B. Konrad, and T. Weser, Vacuum **41**, 449 (1990).
[20]G. Mathieu, R. Contini, J. M. Layet, P. Mathiez, and S. Giorgio, J. Vac. Sci. Technol. A **6**, 2904 (1988).
[21]A. L. Wachs, T. Miller, A. P. Shapiro, and T.-C. Chiang, Phys. Rev. B **35**, 5514 (1987).
[22]T. G. Andersson, G. Le Lay, J. Kanski, and S. P. Svensson, Phys. Rev. B **36**, 6231 (1987).
[23]E. Bauer and J. H. van der Merwe, Phys. Rev. B **33**, 3657 (1986).
[24]E. Bauer, H. Poppa, G. Todd, and P. R. Davis, J. Appl. Phys. **48**, 3773 (1977); P. D. Augustus and J. P. Jones, Surf. Sci. **64**, 713 (1977).
[25]E. Bauer and H. Poppa, Thin Solid Films **121**, 159 (1984).
[26]A. Pavlovska, M. Paunov, and E. Bauer, Thin Solid Films **126**, 129 (1985).
[27]A. Pavlovska and E. Bauer, Surf. Sci. **177**, 473 (1986).
[28]A. Pavlovska, H. Steffen, and E. Bauer, Surf. Sci. **195**, 207 (1988).
[29]G. Lilienkamp, C. Kozioł, and E. Bauer, Surf. Sci. **226**, 358 (1990).
[30]C. Kozioł, G. Lilienkamp, and E. Bauer, Phys. Rev. B **41**, 3364 (1990).
[31]H. Knoppe and E. Bauer, Phys. Rev. B **48**, 1794 (1993).
[32]G. Lilienkamp, C. Kozioł, and E. Bauer, in *Reflection High-Energy Electron Diffraction and Reflection Electron Imaging of Surfaces*, edited by P. K. Larsen and P. J. Dobson (Plenum, New York, 1988), p. 489.
[33]H. Melle and E. Menzel, Z. Naturforsch. **33a**, 282 (1978).
[34]In the case of large film roughness the oscillation period is smaller than the deposition time for one monolayer (Ref. 35).
[35]Z. Mitura and A. Daniluk, Surf. Sci. **277**, 229 (1992).
[36]Z. Mitura, M. Stróżak, and M. Jałochowski, Surf. Sci. Lett. **276**, 15 (1992).
[37]The weak feature at 2 ML and -0.75 eV is due to the He I satellite line (23.09 eV).
[38]W. Jaskólski, V. R. Velasco, and F. García-Moliner, Phys. Scr. **43**, 337 (1991).
[39]The phase depends on the labeling of the well states, compare Ref. 6, and on the definition in Eq. (1), compare Ref. 4. The phases Φ therein are connected with our δ by $\Phi = 2\pi - \delta$.
[40]K. W.-K. Shung and G. D. Mahan, Phys. Rev. B **38**, 3856 (1988).
[41]R. H. Gaylord and S. D. Kevan, Phys. Rev. B **36**, 9337 (1987).
[42]K. Jacobi and P. Althainz, Surf. Sci. **211/212**, 456 (1989).
[43]G. W. Graham, Surf. Sci. **184**, 137 (1987).
[44]J. C. Hansen, M. K. Wagner, and J. G. Tobin, in *Structure/Property Relationships for Metal/Metal Interfaces*, edited by A. D. Romig, D. E. Fowler, and P. D. Bristowe, MRS Symposium Proceedings No. 229 (Materials Research Society, Pittsburgh, 1991), p. 9; B. J. Knapp, J. C. Hansen, J. A. Benson, and J. G. Tobin, Surf. Sci. Lett. **188**, 675 (1987); J. C. Hansen, J. A. Benson, W. D. Clendening, M. T. McEllistrem, and J. G. Tobin, Phys. Rev. B **36**, 6186 (1987).
[45]D. L. Weissman-Wenocur, P. M. Stefan, B. B. Pate, M. L. Shek, I. Lindau, and W. E. Spicer, Phys. Rev. B **27**, 3308 (1982).
[46]G. K. Wertheim, D. N. E. Buchanan, and V. Lee, Phys. Rev. B **34**, 6869 (1986).
[47]M. Salmerón, S. Ferrer, M. Jazzar, and G. A. Somorjai, Phys. Rev. B **28**, 6758 (1983).
[48]J. E. Houston, P. J. Feibelman, D. G. O'Neill, and D. R. Hamann, Phys. Rev. B **45**, 1811 (1992).